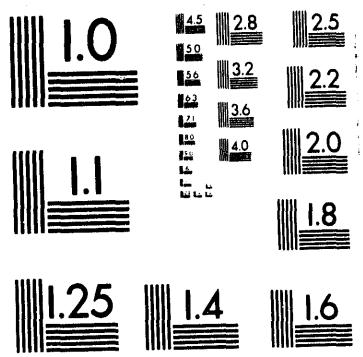
1.0
1.1
1.25
1.4
1.6
1.8
2.0
2.2
2.5
2.8
3.2
3.6
4.0
4.5
5.0
5.6
6.3
7.1
8.0
9.0

1 of 1

ANL/EP/CP--79740-Rev.

REVISED

Conf-930928--3-Rev.

ANALYSIS OF BEAM-ON-TARGET INTERACTION IN A NEUTRON-SOURCE TEST FACILITY*

A. Hassanein and D. Smith
Argonne National Laboratory
9700 S. Cass Avenue
Argonne, IL 60439 USA
Telephone: (708) 252-5889
FAX: (708) 252-5287
EMail: ahmed_hassanein.cmt@qmgate.anl.gov

October 1993

* Work supported by the U.S. Department of Energy, Office of Fusion Energy, under Contract W-31-109-Eng-38.

Presented at the Sixth International Conference on Fusion Reactor Materials, September 27 - October 1, 1993, Stresa, Lago Maggiore, Italy

ANALYSIS OF BEAM-ON-TARGET INTERACTION IN A NEUTRON-SOURCE TEST FACILITY*

A. Hassanein and D. Smith
Argonne National Laboratory
9700 S. Cass Avenue
Argonne, IL 60439
U.S.A.

The need is urgent for a high-flux, high-energy neutron test facility to evaluate the performance of fusion reactor materials. An accelerator-based deuterium-lithium source is generally considered the most reasonable approach to a high-flux neutron source in the near future. The idea is to bombard a high-energy (20-40 MeV) deuteron beam into a lithium jet target to produce high-energy neutrons in order to simulate a fusion reactor environment via the Li (d, n) nuclear stripping reaction.

Deposition of the high-energy deuteron beam and the subsequent response of the lithium jet are modeled and evaluated in detail. To assess the feasibility of this concept, the analysis is done parametrically for various deuteron beam energies, beam currents, and jet velocities. A main requirement for a successful operation is to keep the free jet surface at a minimum temperature to reduce surface evaporation of lithium into the vacuum system. The effects of neutron-generated heating and irradiation on the jet-supporting back plate are also evaluated. The back plate must maintain a reasonable lifetime during system operation.

*Work supported by the U.S. Department of Energy, Office of Fusion Energy, under Contract W-31-109-Eng-38.

I. Introduction

The current understanding of materials behavior in a fusion reactor radiation environment is insufficient to ensure the necessary performance of future fusion reactor components. The need is urgent for a high-flux, high-energy neutron test facility to evaluate the performance of fusion reactor materials. None of the world's existing facilities can reasonably simulate the anticipated neutron environment of a fusion reactor. The strong scientific and technological incentives for understanding materials behavior in such an environment are considered very important. High neutron fluxes corresponding to a wall loading of up to 2 MW/m^2, neutron spectra similar to those exposed to the first wall, and high fluences producing up to 100 dpa in a few years are required to simulate materials condition in a Demo fusion reactor [1].

High-energy neutrons can be produced by stripping the neutron from a deuterium ion during bombardment of a target atom. An accelerator-based deuterium-lithium source similar to that proposed in the original Fusion Materials Irradiation Test (FMIT) facility, Trego [2], Lawrence [3], is generally considered to be the most reasonable approach to a high-flux neutron source in the near future. In this concept, a high-energy (30-40 MeV) deuteron beam is bombarded into a lithium target to produce the high-energy neutrons needed to simulate the fusion environment via the Li (d, n) nuclear stripping reaction. Figure 1 is a schematic illustration of a beam on target interaction assembly in a neutron-source test facility. The neutron spectrum, which peaks near a neutron energy of 14 MeV, produces atomic displacements and transmutation products in irradiated materials under conditions similar to those in real fusion reactors. Lithium is ideally suited as a target material because of the high rate of neutrons produced

Fig 1

during the reaction. The high heat capacity, high thermal conductivity, and low vapor pressure of lithium are also advantageous properties for a coolant. Deposition of the high-energy deuteron beam and the subsequent response of the lithium jet are modeled and evaluated in detail. To assess the feasibility of such a concept, the analysis is done parametrically for various deuteron beam energies, beam currents, and jet velocities. A main requirement for successful operation is to keep the free jet surface at a minimum temperature to reduce the surface evaporation of lithium into the vacuum system. Also evaluated are the effects of neutron generated heat and irradiation effects on the back plate that supports the jet. The back plate must maintain a reasonable lifetime during the operation of the system.

II. Beam-on-target interaction

The deposition and the response of the lithium jet due to the bombardment of high-energy deuterons are modeled and simulated with the A*THERMAL computer code, Hassanein [4]. The code is modified to handle the deposition of high-energy ions in different target materials. Using different analytical models, the code calculates the energy loss of the incident ion beam through both the electronic and nuclear stopping powers of the target atoms along its path. The analytical models use stopping cross sections that incorporate experimental data for accurate modeling of the deposition profile. This code is much faster and more reliable than Monte Carlo codes, which require extensive running time and careful statistical interpretation of the results. A brief description of the models used in calculating the beam deposition is provided below.

An ion beam traveling through matter loses energy primarily due to ionization and excitation of the electron cloud surrounding the nucleus. At low particle energy, elastic nuclear scattering can also result in an appreciable energy loss. This is particularly important near the end-of-range where the deposited energy reaches a peak. For nonrelativistic ions, the general Bethe equation is used to describe the bound-electron stopping power and has the form, Jackson [5]

$$\frac{dE}{dx} = \frac{4\pi N_o Z_{eff}^2 \rho e^4 Z_2}{m_e c^2 \beta^2 A_2} \left[\ln\left(\frac{2 m_e c^2 \beta^2 \gamma^2}{\dot{I}} \right) - \beta^2 - \sum_i c_i / Z_2 \right], \qquad (1)$$

where Z_{eff} = effective charge of the projectile ion, N_o = Avogadro's number, ρ = density of the stopping medium, A_2 = atomic weight of the stopping medium, Z_2 = atomic number of the stopping medium, β = (particle velocity)/c, c = velocity of light in vacuum, m_e = electron rest mass, $\dot{I}$ = average ionization potential, $\sum c_i / Z_2$ = sum of the effects of shell corrections on the stopping charge, and e = electronic charge.

For low-energy ions, the Bethe theory is not appropriate and instead the Lindhard model is used. This model uses a Thomas-Fermi description of the ion and stopping-atom electron clouds that are due not only to excitation and ionization of the stopping atoms, but also due to elastic Coulomb collisions of the ion and the nucleus of the stopping atom. The electronic stopping power is given by, Lindhard [6]

$$\frac{dE}{dx} = C_{LSS} E^{1/2}, \qquad (2)$$

where C_{LSS} is a constant that depends on both the incident ion and the target material parameters.

Nuclear stopping due to elastic Coulomb collisions between the ion and the target nuclei becomes significant at very low ion energies. An expression for nuclear stopping is given by, Lindhard [7]

$$\frac{dE}{dx} = \rho C_n E^{1/2} \exp\left[-45.2(C_n' E)^{0.277}\right], \tag{3}$$

where

$$C_n = \frac{4.14\times10^6}{A_1^{1/2}}\left(\frac{A_1}{A_1+A_2}\right)^{3/2}\left(\frac{Z_1Z_2}{A_2}\right)^{1/2}\left(Z_1^{2/3}+Z_2^{2/3}\right)^{-3/4}, \tag{4}$$

$$C_n' = \frac{A_2}{(A_1+A_2)}\frac{1}{Z_1Z_2}\left(Z_1^{2/3}+Z_2^{2/3}\right)^{-1/2} \tag{5}$$

The total stopping power for an ion slowing down in the target material is given by taking the minimum of either the Bethe (Eq. 1) or Lindhard (Eq. 2) electronics stopping power and then adding to it the above nuclear stopping power (Eq. 3).

The code then calculates the detailed thermal response of the jet and the supporting back plate, subject to various boundary conditions. The code uses both finite-element and finite-difference methods with advanced numerical techniques for high accuracy and efficient solution. Models to calculate net surface evaporation rate of the Li jet are also implemented in the code, Hassanein [4].

III. Li jet response

Figure 2 shows an energy-loss profile of a deuteron beam incident on a Li jet with various monoenergetic initial beam energies. The deuteron energy range in Li decreases substantially as incident energy decreases. The range of deuteron ions in the Li target have a dependence slightly lower than E^2 . Varying the initial deuteron energy may be desirable to produce neutron spectra with different characteristics for a wide range of nuclear applications, Noda [8]. A finite spread in the deuteron beam's incident energy can significantly reduce peak energy deposition near the end of the range. The beam produced by an accelerator is usually not monoenergetic, but has a Gaussian energy distribution with a low RMS, σ, value.

Figure 2 also shows the effect of a small spread in beam energy on the peak energy deposited inside the Li jet. A Gaussian profile of only $\sigma = \pm 0.5$ MeV can reduce the peak energy deposited by a factor of >4. This is particularly important in reducing the Li peak temperature rise near the end of the beam range inside the jet. Figure 3 shows the spatial temperature distribution (x-direction) of the jet for both a Gaussian and a monoenergetic beam. The calculation shown is for a beam size of 1 x 3 cm^2 in the y-z plane respectively (see Fig. 1) and for 100 mA beam current. This maximum temperature shown is for the locations y = 1 in the x-y plane at the end of the jet exposure. A Gaussian beam with $\sigma = 0.5$ MeV results in a much lower peak temperature, (>400 K lower than that of a monoenergetic beam). This will further increase the margin for no-boiling criteria near the end-of-range for these conditions. However, different beam profiles have little effect on maximum surface temperature. Higher jet velocities, however, are found to significantly decrease both the temperature profile inside

the jet and the surface temperature. The jet flow profile is assumed to be laminar. With proper nozzle design the flow characteristics can be somewhat controlled. Turbulent flow will increase flow mixing, which will tend to decrease the peak temperature rise inside the jet and increase the surface temperature.

Recently, it was recommended the use of larger beam sizes with higher beam current to ensure reasonable test volumes. Larger test volumes are important for determining meaningful radiation damage analysis and for both mechanical and thermophysical property testing experiments. Figure 4 shows the Li maximum temperature distribution inside the jet for different beam sizes and beam currents. Higher beam currents always result in more power deposited and consequently higher jet temperatures. Larger beam sizes result in lower power densities and lower jet temperatures. For the same beam area and beam current, the shorter the beam size in the flow direction (y-direction) the lower the jet maximum temperature.

Lower jet surface temperature is very important in reducing the evaporation rate into the vacuum chamber and into the accelerator. A higher Li flux evaporated from the surface can interfere with the incoming deuteron beam and can activate various components of the accelerator. In addition, this Li flux can be a major burden on the vacuum system. Figure 5 shows the Li jet surface temperature along the flow (y-direction) and the corresponding vaporization rate for different beam sizes and currents. The vaporization rate is calculated only for an area equal to the beam size and assuming 100% duty factor. It is expected, however, that the exposed jet area will be larger than the beam size. This is particularly important downstream, where the surface temperature does not drop immediately due to thermal diffusion from the bulk to the surface. As a result, the

actual vaporization rate can be much higher. A slight increase in surface temperature can substantially increase the net Li erosion rate.

Figure 6 shows the effect of different beam energies on the jet surface temperature and the resulting vaporization rate. Lower beam energies, which deposit more energy near the surface, result in much higher surface temperatures and orders-of-magnitude higher Li vaporization rates. Lower beam energies may have to be accommodated by higher jet velocities, lower beam currents, or larger beam sizes in order to reduce surface vaporization.

Several other issues related to performance of the high-velocity jet must be considered in detail in future studies. Erosion of the structure and in particular the jet nozzle may cause flow instabilities at the jet surface and shorten the nozzle lifetime. The effect of possible Li jet boiling on the dynamic behavior and on the stability of the jet needs to be investigated in detail. Sputtering of Li atoms from the surface jet by the deuteron beam is, however, calculated to be very small compared to thermal emission. Effect of beam momentum delivered to the Li jet is also expected to be small.

IV. Response of back plate

A major reason for using the curved back plate behind the jet is to increase the pressure jet internally and thus prevent local boiling at the location of peak deuteron energy deposition. The back plate may also help to stabilize the jet and establish a vacuum boundary between the jet and the test area. Significant energy will be deposited within the plate due to neutron deposition and resulting γ-rays; most of this energy is transferred by conduction to the flowing lithium at

the inner surface of the plate. Both the temperature rise inside the plate and the resulting neutron damage will determine plate lifetime. The plate must have a reasonable lifetime in order to maintain uninterrupted operation and ensure economic feasibility. Thermal response of the plate from nuclear heating is discussed below. The nuclear response and the resulting damage are described elsewhere in this proceedings volume, Gomes [9]. Figure 7 shows the temperature distribution in a stainless steel back plate at different beam parameters. Higher beam currents result in more nuclear heating inside the plate and consequently a higher temperature rise. Lower plate temperatures are desired in order to reduce and mitigate the effect of neutron damage (such as swelling) on plate lifetime. Figure 8 shows a comparison of stainless steel and vanadium as back-plate materials. Vanadium results in a lower temperature rise, for two main reasons: (a) vanadium has better thermal conductivity than stainless steel and (b) total nuclear heat generated is lower in vanadium than in stainless steel. Figure 8 also shows that thinner back plates result in a lower temperature rise because the total nuclear heat generated is lower than that in thicker plates. Back-plate thickness will be determined by several factors such as jet mass flow rate, neutron damage, and overall design requirements.

Fig 7

Fig 8

V. Conclusions

A beam on target interaction assembly for an accelerator-based deuterium-lithium neutron source is analyzed and evaluated. Deuteron energy deposited and the resulting Li target heating calculations seem to be manageable up to beam currents of 250 mA. Surface evaporation from the Li jet depends on beam size, beam current, beam energy, and jet velocity. Larger beam sizes reduce the thermal load inside the jet and increase the available test volume. Thermal loads

in the back plate appear to be more tolerable with thinner plates. Other issues such as beam stability at higher velocities, erosion of the structure by the flowing jet, and maximum allowable jet surface evaporation require study.

VI. References

[1] "A Demonstration Tokamak Power Plant Study - Demo," ANL/FPP/82-1, Argonne National Laboratory, September 1982.

[2] A.L. Trego et al., "Fusion Materials Irradiation Test Facility - A Facility for Fusion Materials Qualification," Nucl. Tech. Fusion, 4 (2) (1983) 695.

[3] G.P. Lawrence et al., J. Fusion Energy, 8 (3/4) (1989) 201.

[4] A. Hassanein, J. Nucl. Mater., 122 & 123 (1984) 1453.

[5] J.D. Jackson, Classical Electrodynamics (Wiley, 1975).

[6] J. Lindhard, M. Scharff, and H.E. Schiott, K. Dan. Vidensk, Selsk. Mat. Fys. Medd., 33 (14) (1963).

[7] J. Lindhard and M. Scharff, Phys. Rev., 124 (1964) 128.

[8] K. Noda et al., J. Nucl. Mater., 179-181 (1991) 1147.

[9] I.C. Gomes and D.L. Smith, these proceedings.

Figure Captions

Figure 1 Schematic illustration of beam on target interaction assembly in a neutron-source test facility.

Figure 2 Energy-loss profile of deuteron beam in Li target.

Figure 3 Spatial distribution of Li maximum temperature for Gaussian and monoenergetic beam profiles.

Figure 4 Spatial distribution of Li maximum temperature for different beam sizes and currents.

Figure 5 Jet surface temperature and vaporization rate at different beam sizes and currents.

Figure 6 Jet surface temperature and vaporization rate at different beam energies.

Figure 7 Spatial distribution of stainless steel back-plate temperature at different beam parameters.

Figure 8 Back-plate temperature distribution for stainless steel (SS) and vanadium (V) plates at different plate thicknesses.

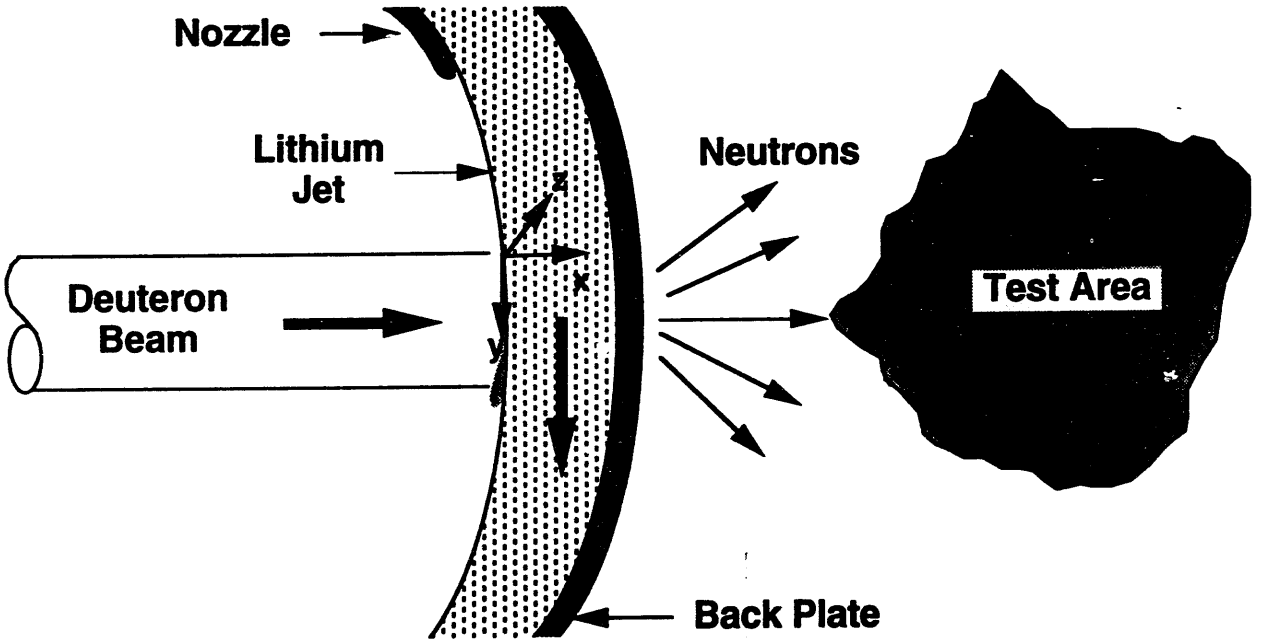
Nozzle
Lithium Jet
Deuteron Beam
z
x
y
Neutrons
Test Area
Back Plate

Fig ①

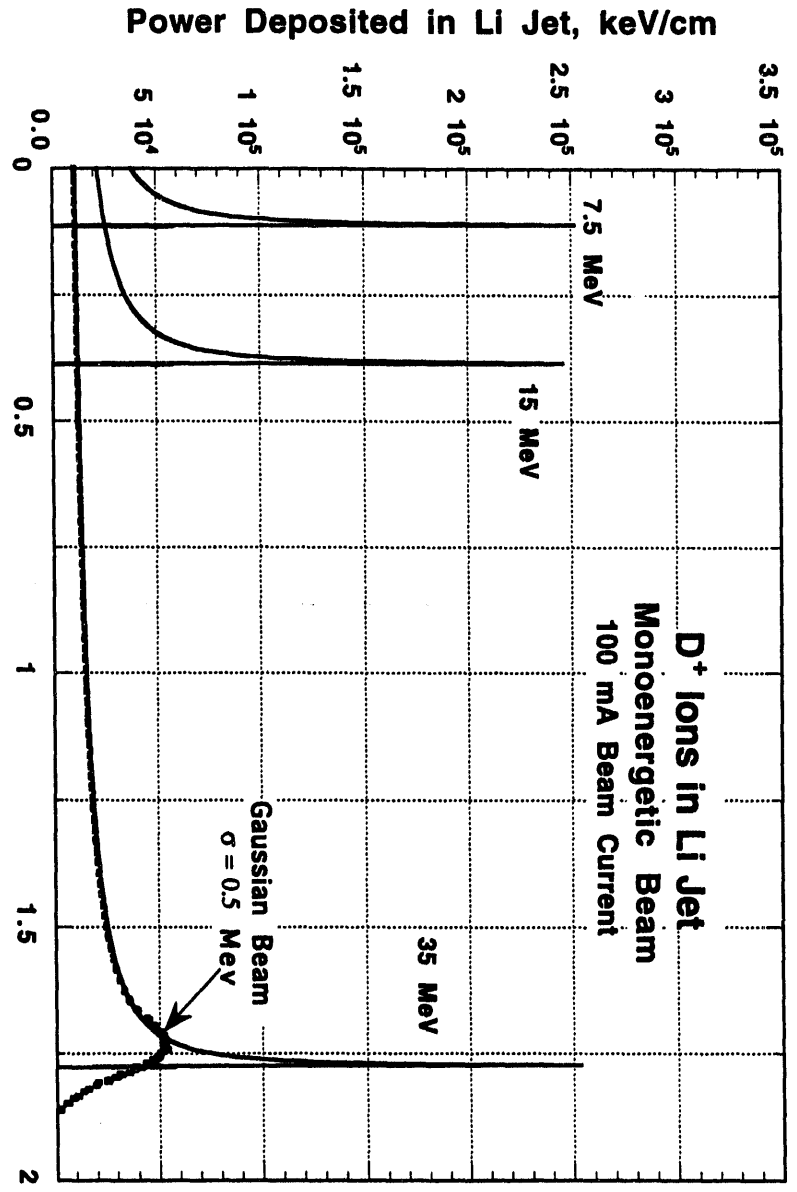
Power Deposited in Li Jet, keV/cm
3.5 10^5
3 10^5
2.5 10^5
2 10^5
1.5 10^5
1 10^5
5 10^4
0.0 0
0.5
1
1.5
2
Distance in Li Jet, cm
D+ Ions in Li Jet
Monoenergetic Beam
100 mA Beam Current
7.5 MeV
15 MeV
35 MeV
Gaussian Beam
σ = 0.5 Mev

Fig ②

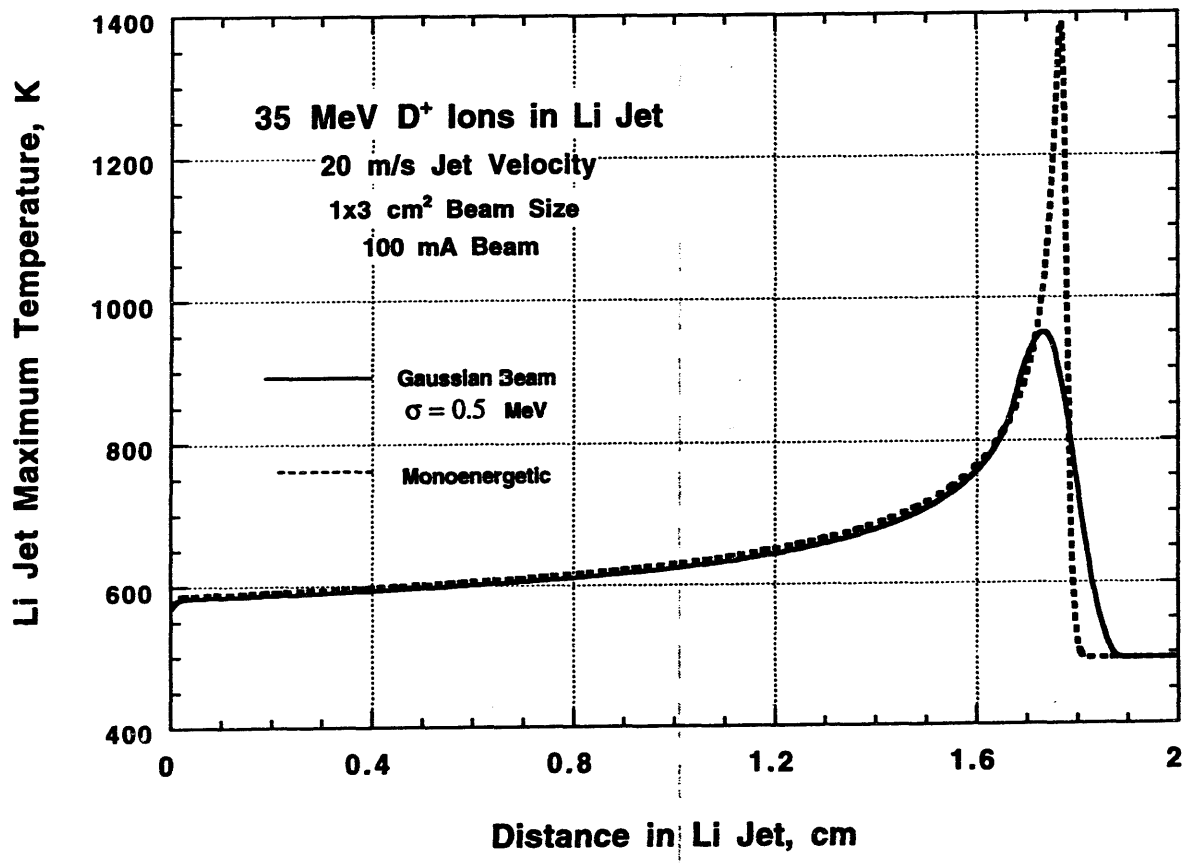
35 MeV D+ Ions in Li Jet
20 m/s Jet Velocity
1x3 cm2 Beam Size
100 mA Beam
Gaussian Beam
σ = 0.5 MeV
Monoenergetic
Li Jet Maximum Temperature, K
Distance in Li Jet, cm
1400
1200
1000
800
600
400
0
0.4
0.8
1.2
1.6
2

Fig (3)

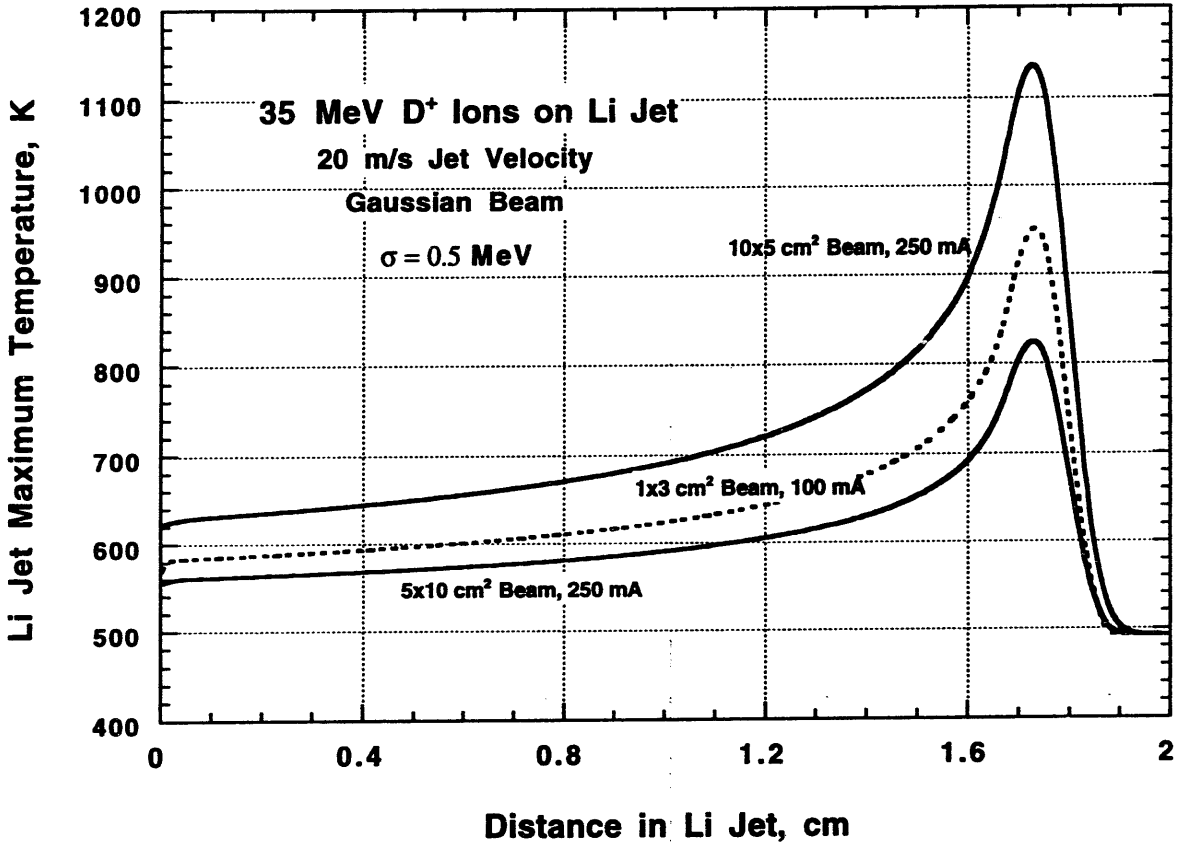
35 MeV D+ Ions on Li Jet
20 m/s Jet Velocity
Gaussian Beam
σ = 0.5 MeV
10x5 cm² Beam, 250 mA
1x3 cm² Beam, 100 mA
5x10 cm² Beam, 250 mA
Li Jet Maximum Temperature, K
Distance in Li Jet, cm
1200
1100
1000
900
800
700
600
500
400
0
0.4
0.8
1.2
1.6
2

Fig ④

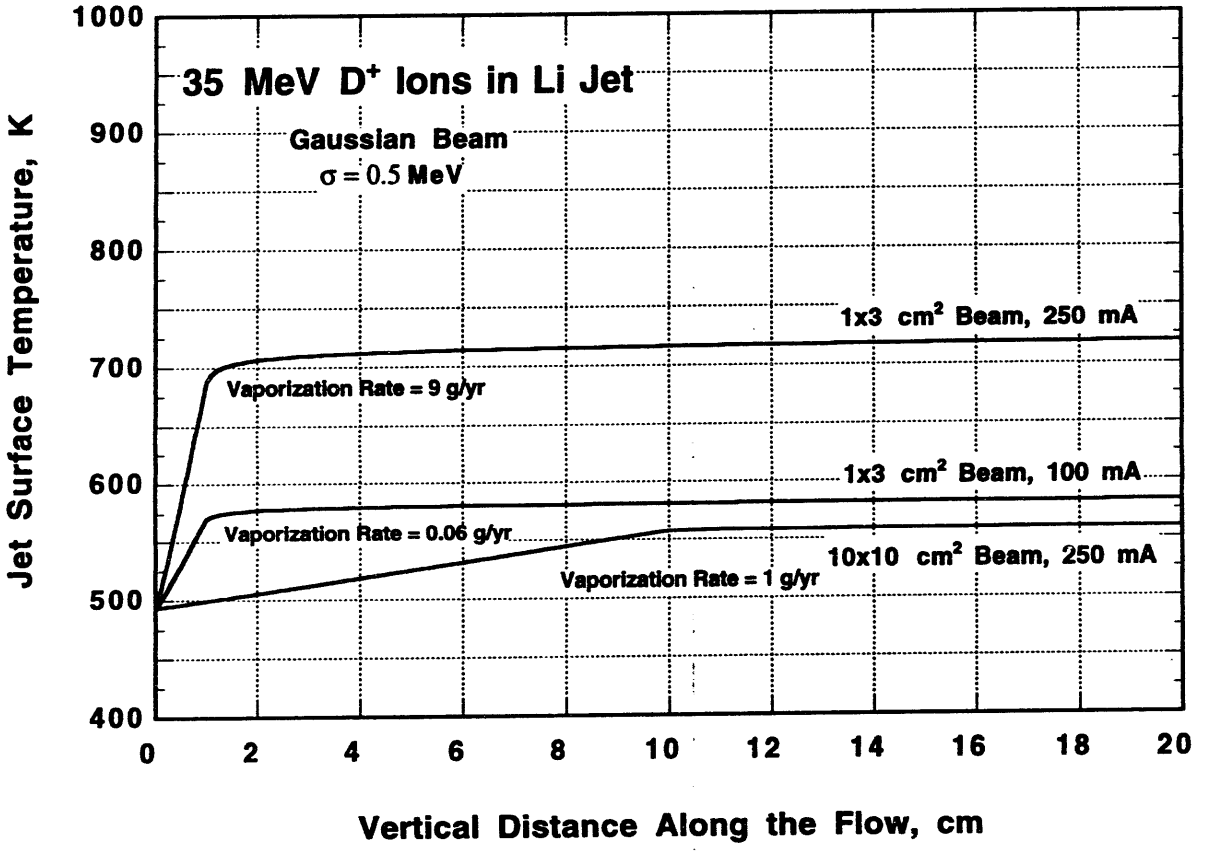
35 MeV D+ Ions in Li Jet
Gaussian Beam
σ = 0.5 MeV
1x3 cm² Beam, 250 mA
Vaporization Rate = 9 g/yr
1x3 cm² Beam, 100 mA
Vaporization Rate = 0.06 g/yr
10x10 cm² Beam, 250 mA
Vaporization Rate = 1 g/yr
Jet Surface Temperature, K
Vertical Distance Along the Flow, cm
1000
900
800
700
600
500
400
0
2
4
6
8
10
12
14
16
18
20

Fig ⑤

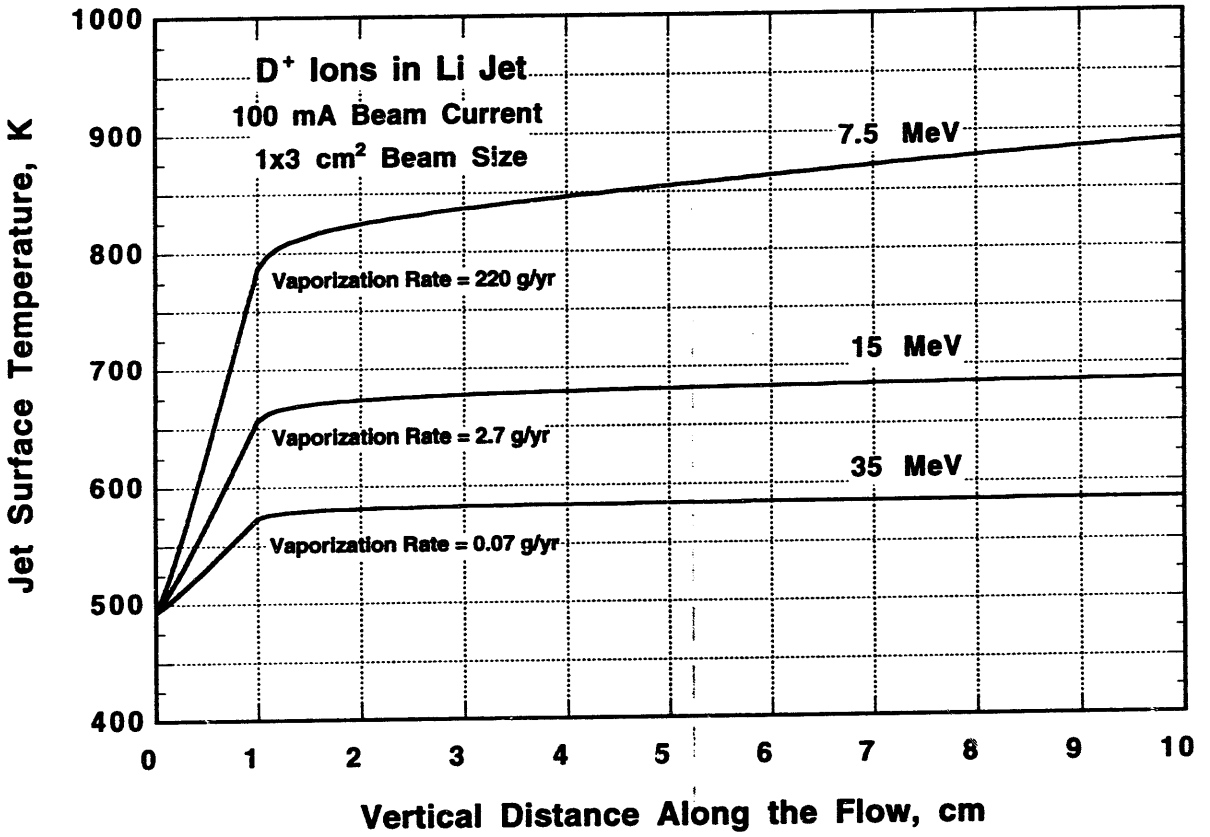
D+ Ions in Li Jet
100 mA Beam Current
1x3 cm2 Beam Size
7.5 MeV
15 MeV
35 MeV
Vaporization Rate = 220 g/yr
Vaporization Rate = 2.7 g/yr
Vaporization Rate = 0.07 g/yr
Jet Surface Temperature, K
Vertical Distance Along the Flow, cm
1000
900
800
700
600
500
400
0
1
2
3
4
5
6
7
8
9
10

fig ⑥

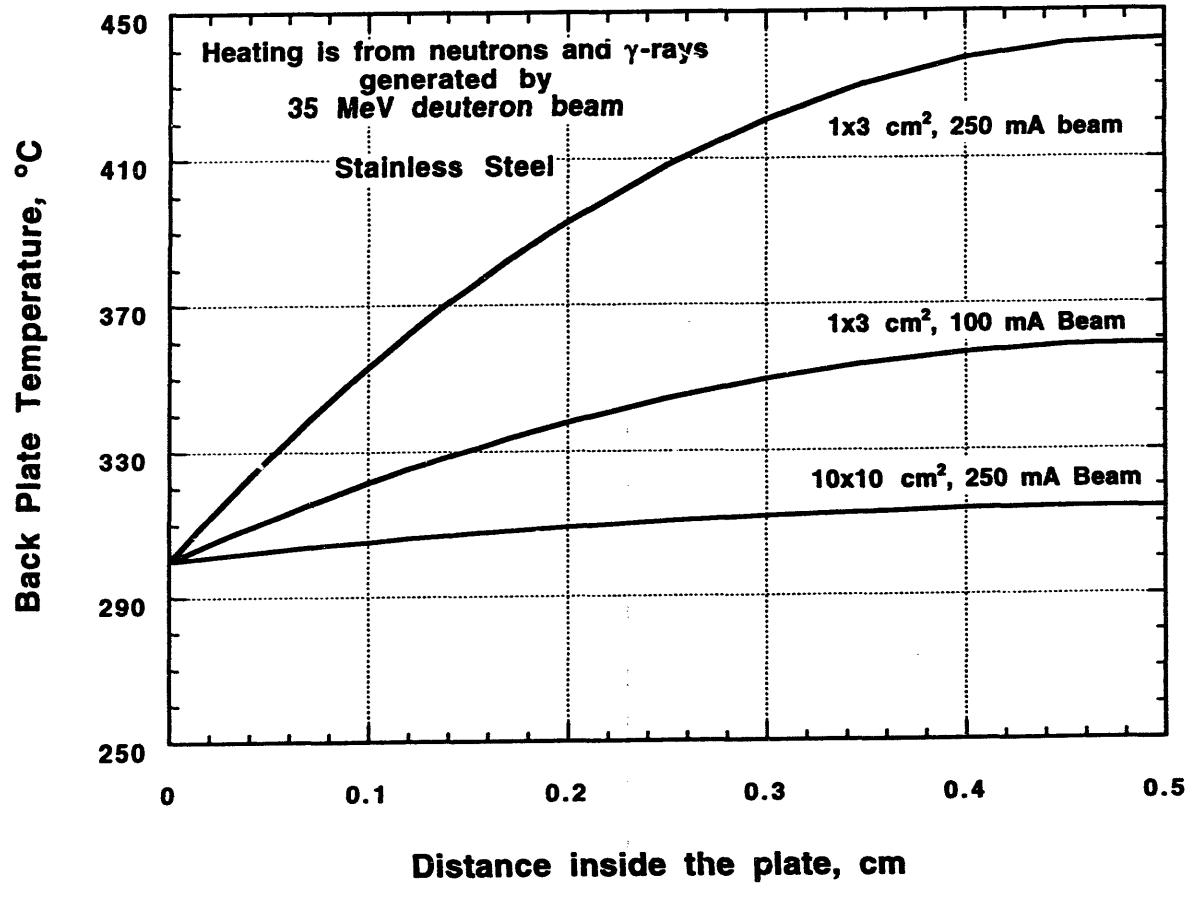
Heating is from neutrons and γ-rays
generated by
35 MeV deuteron beam
Stainless Steel
1x3 cm², 250 mA beam
1x3 cm², 100 mA Beam
10x10 cm², 250 mA Beam
Back Plate Temperature, °C
450
410
370
330
290
250
0
0.1
0.2
0.3
0.4
0.5
Distance inside the plate, cm

fig (7)

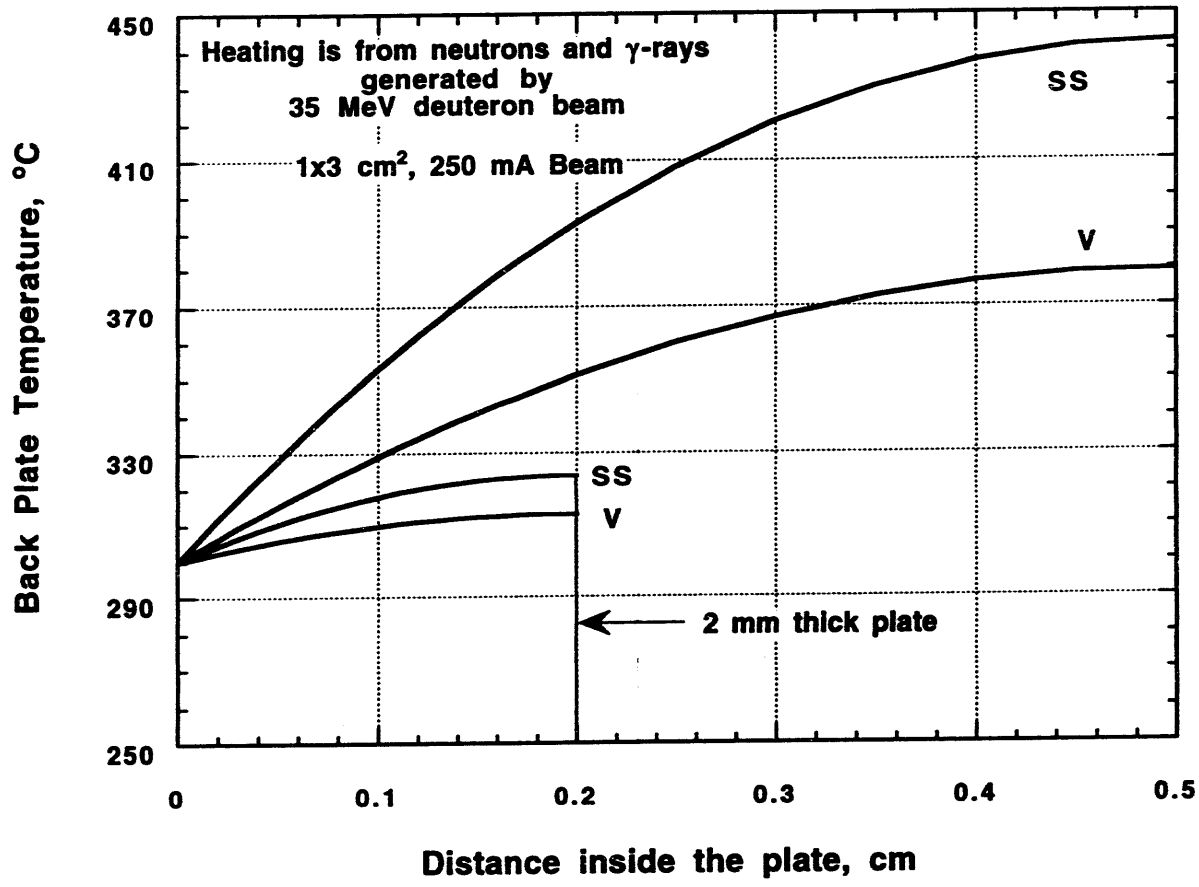
Heating is from neutrons and γ-rays
generated by
35 MeV deuteron beam
1x3 cm², 250 mA Beam
SS
V
SS
V
2 mm thick plate
Back Plate Temperature, °C
450
410
370
330
290
250
0
0.1
0.2
0.3
0.4
0.5
Distance inside the plate, cm

Fig (8)

DATE

FILMED

2/22/94

END